31st Annual International Conference of the IEEE EMBS
Minneapolis, Minnesota, USA, September 2-6, 2009

# Inductive Link Design for Miniature Implants

Philip R. Troyk, *Senior Member, IEEE*, Alexander D. Rush

***Abstract*—Advances in microfabrication have allowed the integration of large numbers of electrodes onto one platform. The small size and high channel density of these microelectrode arrays which promise improved performance of a neural prosthesis also complicate the design of an inductive link to achieve efficient powering and communication with the implant. Stimulating or recording with many channels requires high data rate transmission. At the same time, power must be transmitted to the implanted device without exceeding power dissipation limits within the body. Using conventional design techniques, achieving all of these competing requirements simultaneously can require many time consuming iterations. It is proposed that a transcutaneous power and data link can be optimized to meet system level design parameters (power dissipation, data rate, secondary voltage, etc.) by having an analytic understanding of the interacting link level design parameters (receiver radius, carrier frequency, number of turns, implant location, etc.). We demonstrated this technique with the design of a transcutaneous power and data link for an intracortical visual prosthesis.**

## I. Introduction

Recent studies have demonstrated the promise of developing neuroprosthetic devices to restore lost motor and sensory function using neural recording and stimulating arrays. However, for long-term daily use of a neural prosthesis neural data must be transmitted wirelessly out of the body, because wires crossing the skin have an excessive risk of infection and breakage and are often considered highly unaesthetic by the volunteer [1-6].

Despite the success of prototype prostheses controlled by neural signals, a combined efficient power and high data rate outward telemetry link remains a serious obstacle to the clinical and commercial availability of a high channel-count motor prosthesis as is evident by the large number of publications addressing this issue.

It is generally accepted that the performance of a neural prosthesis will increase with channel count, whether the goal is stimulation (e.g. cochlear prosthesis, visual prosthesis, functional electrical stimulation) or recording (e.g. cortical neuromotor prosthesis, EMG controlled hand prosthesis). However, this also results in increased competition between power and data rate requirements.

As the design of neuroprostheses continues to experience a growth in channel density and complexity, there is a growing need for high bandwidth transcutaneous bidirectional data transmission (>1Mbps). High bandwidth data transmission is costly not only in terms of power consumption, but also with respect to maintaining strict limitations on power density within the body (<80mW/cm$^2$ [7]) in order to avoid tissue damage. Power dissipation results from losses in both the implanted circuitry and in the implanted coil(s).

Anatomy can also strictly limit the size of the implanted device. In addition to imposing low power dissipation limits, the small size of the implant makes delivering the required power difficult due to the resultant low coupling between the external and implanted coils. The low coupling coefficient is often further reduced by the need for a large anatomy-defined separation between the transcutaneous coils. Our recent surgical in-vivo experiences for the Intracortical Visual Prosthesis have led us to conclude that cables crossing the dura may pose considerable risk of infection [8] or cerebrospinal fluid leakage, and for cortical neural prosthesis with many channels, the safest intracortical implant design is fully contained beneath the dura. Unfortunately this means a separation of roughly 20mm between the face of the external coil and the implanted coil (≈8mm maximum for scalp [9], ≈11mm maximum for skull [10], and some small separation due to dura and cerebrospinal fluid [11]). Such a design could also be considered for other neural prostheses which require many channels, such as an intracortical neuromotor prosthesis.

Inductive power transmission is often achieved by using a power amplifier (PA) to resonate an LC circuit thus creating high AC current, and producing a magnetic field which is received by the implanted coil. The implant coil is part of a parallel tank circuit, driven at resonance, to produce a high AC voltage, which is rectified to produce the supply voltage, as illustrated in Fig. 1.

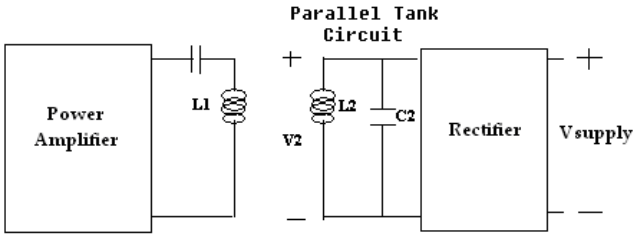


Fig. 1. Inductive Power Transmission System

A number of papers have been published with methods to optimize inductive power and data links, including those found in [12-19]. These methods are sometimes qualitative and sometimes quantitative in nature. The focus of these papers, however, has been to maximize the efficiency of the link, while neglecting other concerns, such as bandwidth (BW), self-resonant frequency (SRF), power dissipation, etc. Using conventional design techniques, achieving all of these competing requirements simultaneously can require many time consuming iterations. Our premise is that the transcutaneous link can be optimized to system level design parameters (power dissipation, data rate, secondary voltage, etc.) by having an analytic understanding of the different link-level design parameters (receiver radius, carrier frequency, number of turns, implant location, etc.), combined with an understanding of how they interact.

## II. Procedure and Methods

### A. Optimization

A number of link-level design parameters affect the performance of the transcutaneous link. The complexity of transcutaneous link design results from the interdependence of these parameters and the tradeoffs between competing design goals. The design parameters and their interaction are illustrated in Fig. 2.

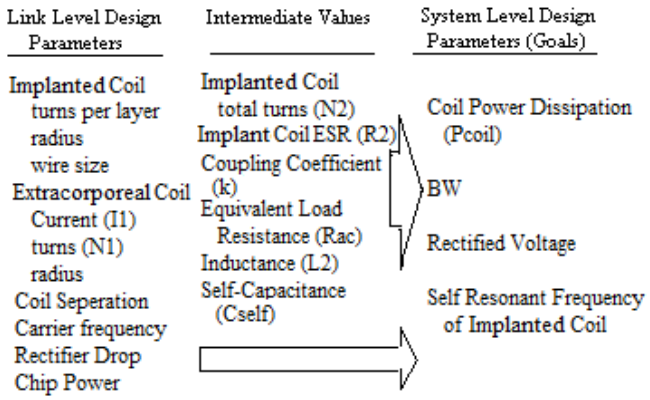


Fig. 2. Illustration of Design Parameters and their Interaction

As a consequence of design parameter interactions and tradeoffs between multiple design goals, simplistic design techniques are often insufficient. For the example of the intracortical visual prosthesis transcutaneous link, if one merely uses a small number of turns on the implant coil, then coil losses become greater than power delivered to the load, making the rectified voltage too low to operate the chip, while the coil losses exceed the limitations to prevent tissue damage (in addition to a prohibitively low BW). If one chooses to use the maximum turns as allowed by coil winding cross section, then current delivered to the inductively coupled receiver is too low due to its high impedance.

Due to the inadequacy of simplistic design techniques, we chose to create a multiparametric analytic model of the transcutaneous link to allow a simple iterative optimization of the link, i.e. brute force optimization.

### B. Design Parameters and Their Interaction

#### 1. Calculating Secondary Voltage

An expression for voltage across the implanted coil, i.e. the secondary voltage, as a function of the link parameters has been given by [9] for miniature implanted coils. However, this derivation is for a series resonant transmitter tank with assumptions that are often not valid e.g. ($R_1R_2>>k^2L_1L_2w^2$). In addition, the expression is in terms of link parameters which cannot be typically manipulated independently such as inductance and effective series resistance, ESR, in contrast to turns per layer, number of layers, wire diameter, etc., which can be directly manipulated. Therefore, we derived an expression for the secondary (implant side) voltage and combined this with expressions for the interdependent link parameters (e.g. inductance, ESR, etc.) in terms of the independent link parameters (e.g. turns per layer, number of layers, average receiver radius, etc.).

Below is the equivalent secondary circuit using the method described in Radio Engineer's Handbook [20]:

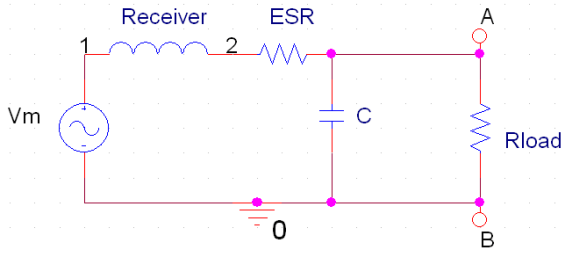


Fig. 3. Equivalent Secondary Circuit from [14]

$$V_m=I_1(j\omega L_m)=j\omega k\sqrt{L_1L_2}\,I_1 \quad (1)$$

where $I_1$ is the current in the extracorporeal coil, k is the coupling coefficient, $L_1$ is the inductance of the extracorporeal coil, $L_2$ is the inductance of the implant, $L_m$ is the mutual inductance, and $\omega$ is the angular carrier frequency.

Using Norton Equivalent Circuit we computed an expression for the implanted coil voltage, $V_2$, as a function of the link parameters which typically agreed with simulation results to within 1%. Due to its complexity we have not included this equation here.

#### 2. Calculating the Coupling Coefficient

The coupling coefficient is a value between 0 and 1, which expresses the degree of electrical coupling between the implanted and extracorporeal inductors. This value is an important factor in determining the maximum distance at which correct operation of the implant can be achieved.

The external transmitter coil is generally a single layer coil with a diameter much larger than that of the receiver coil, wound with Litz wire. The advantage of a single layer is a higher self-resonant frequency compared to multiple layers. The required inductance can generally be achieved with only one layer because there are few constraints on the dimensions of the coil outside the body. The advantage of a large diameter is better axial displacement tolerance as well as a less rapid decline in the magnetic field with transmitter to receiver distance.

An expression for the coefficient of coupling, k, is given by [15]. However, this equation assumes that the transmitter and receiver are located in the same plane. The transmitter/receiver separation may be large enough for this assumption to be false. Therefore, the expression for the magnetic field intensity as a function of distance from [21] can be used to calculate k for coaxial, non-coplanar coils (note: this equation assumes that the wire radius is much less than the coil radius) in the same manner as the expression for k in [15]. If the depth of the receiver windings is much less than the average receiver radius and the receiver length is much less than the transmitter length then the magnetic field is relatively constant over all of the windings k can be calculated as follows:

$$k=\frac{\mu\pi R_r^2 N_t N_r}{2L_t\sqrt{L_t L_r}}\left[\frac{d+L_t}{\{(d+L_t)^2+R_t^2\}^{1/2}}-\frac{d}{(d^2+R_t^2)^{1/2}}\right] \quad (2)$$

where $L_r$ is receiver length, $L_t$ is transmitter length, $R_r$ is the average receiver radius, $R_t$ is the transmitter radius, and d is the distance between the face of the transmitter and the central winding of the receiver.

If the assumptions of the above equation are not met, the mutual inductance of transmitter, receiver pairs of almost any dimensions and separation can be given with good accuracy (often within 1%) by the equations given in [22]. For non-coaxial coils, far more complicated equations are given by [15, 21], which take into account axial misalignment.

*3. Calculating the ESR of the implanted coil*

The Effective Series Resistance (ESR) of the receiver is an important factor in determining the AC voltage produced at the rectifier as well as the power dissipated in the implanted coil, which must be limited to prevent tissue damage due to chronic temperature elevation.

The value of ESR is a function of not only the length of wire, but is also increased by current crowding resulting from the skin effect and the proximity effect. Skin effect is the phenomenon of electrons flowing primarily at the surface of an inductor resulting in an increase in its effective series resistance. Current crowding results from eddy currents induced in nearby conductors by an alternating magnetic field which alter the distribution of current flowing through them, such as in a tightly wound coil. In this case, the area of wire in which electrons flow is further crowded, resulting in a much more severe increase in ESR. These phenomena have also been described by in equations developed by [20, 23].

We calculated the AC resistance as given by the Dowell method [23].

[24] showed using finite-element analysis that this method is accurate within 5% as long as the diameter is less than the skin thickness, as is the case for 50AWG, the smallest wire which can realistically be handled for coil winding without breaking, at 5MHz, the power carrier frequency used.

*4. Calculating Receiver Inductance*

Exact inductance values can be determined for a multilayer inductor using complicated formulas, but in the interest of reducing computation time, simpler approximate formulas have been developed. Although these approximate formulas were originally necessitated by the lack of fast computations now provided by calculators and computers, these formulas are surprisingly accurate and are still widely used for the design of inductors. They also have the benefit of reducing the computation time of algorithms which perform inductance calculations repeatedly. The most common formula used to compute the inductance of a multilayer coil of rectangular cross section was provided by [25]. Although this formula is used today to compute the inductance of coils with various radii, axial thickness, and radial thickness combinations it is only guaranteed accurate by the author for the case when the parameters are roughly equal.

A more appropriate formula for the coils we plan to design is provided in [26] and is designed to be accurate for our case when radial thickness and axial thickness are both small in comparison to radius. This approximate formula for inductance is as follows:

$$L=\frac{4\pi N_2^2 a^2}{0.2317a+0.44b+0.39c} \quad (3)$$

in which a- mean radius

b- axial depth

c- radial depth

where the parameters are in cm and the output is in nanoHenries. Parameter a is the radius, b is the axial breadth, and c is the radial depth.

*5. Calculating BW*

The BW of a steady state RLC tank, viewing it as an RLC bandpass filter is given by f/Q, which, for a parallel RLC tank is given by the equation below. Q is the quality factor of the receiver coil, which for a parallel RLC tank is $R/\omega L$. This equation is an approximation, because it assumes that the tank is being driven by an AC current source, which is constant in amplitude with frequency. In actuality, the RLC network is driven by the mutual inductance with an AC amplitude that varies with frequency. This is illustrated by Fig. 3. However, for high values of receiver coil Q (equal to $\omega L_2/R_2$), we have observed good agreement between this equation and the BW observed in simulation (often within 2%).

$$BW=\frac{f_c}{Q}=\frac{1}{2\pi RC} \quad (4)$$

Often the coil resistance cannot be neglected from this computation and the series to parallel resistance should be computed to give the following value of R:

$$R = R_p // R_L$$

$$R_p = (Q^2 + 1)R_2$$

Although it is conventional to say that data rate should be limited to the BW of the RLC tank to avoid intersymbol interference and distortion (for rectangular pulse shaping) when using binary ASK and PSK, a more complex determination of maximum data rate may be required depending on the modulation and demodulation technique.

*6. Calculating the self-capacitance of the receiver*

The self capacitance, $C_{self}$, of the receiver coil, caused by capacitance between the windings and layers of the receiver, together with its inductance value determine the maximum operating frequency of the link, also know as the self-resonant frequency (SRF). $C_{self}$ can be difficult to determine accurately, and is an area of ongoing research. However, self-capacitance can be determined to a reasonable approximation by formulas from [27].

For single layer coils, the $C_{self}$ is computed as the series combination of the wire-to-wire capacitance. For multilayer coils, the layer-to-layer capacitance dominated.

7. Calculating the Equivalent AC Resistance of the Rectifier

To find the equivalent ac resistance of the rectifier, we used the method presented in [27] and [29] except without ignoring the voltage drop of the diodes, which is not negligible for such a low rectified voltage. The power dissipation in the dc load was equated to the power dissipation in the equivalent AC load resistance, $R_{ac}$, which yields the following expression:

$$R_{ac} = \frac{(V_{dc} + 2V_{diode})^2}{2V_{dc}^2} R_{dc} \quad (5)$$

where $R_{dc}$=(Rectified Voltage)/(Current Drawn by Chip).

8. Calculating Power Dissipation in the Implant Coil

According to [7], power dissipation within the body is limited to 80mW/cm$^2$. This value is supported by [30], who found a observed a slightly threshold in cat cortical tissue. The visual prosthesis has a footprint of roughly 0.08cm$^2$, which limits its power dissipation to 6.4mW. Because the implant draws as much as 2.3mW, the coil power dissipation, $P_{coil}$, should be limited to 4.1mW to avoid tissue damage.

The following equation was used to calculate $P_{coil}$.

$$P_{coil} = \frac{1}{2} I_{ac\,coil}^2 R_2 = \frac{1}{2} \frac{V_2^2}{(\omega L_2)^2 + R_2^2} R_2 \quad (6)$$

This expression agreed well with simulation (often within 10%).

## III. Results and Discussion

### A. Empirical Testing of the Link Model

The goal of RF magnetic transcutaneous powering is to achieve at least the required rectified supply voltage at the required distance. Therefore, we tested how well the analytic description of the inductive link could predict the distance at which the minimum rectifier voltage is achieved using a 16 channel implantable stimulator chip as the load. To the best of the authors' knowledge such a prediction has not been reported previously for inductive link design for miniature implants based solely on the independent link-level design parameters. The ability to do so allows automated link design as well as a greater ability to explore the limitations of such a link. A Class E transmitter was used in both cases. The transmitter coil had an inductance of 5μH and carried a current of 0.75A. The radius of all of the implant coils below was 2.26mm.

First, the link model was tested using a four diode rectifier built from discrete signal diodes (Tables I and II). These diodes had a drop of 0.54V with 3.5V across a load resistance of 15kΩ.

TABLE I. Comparison of Predicted and Observed Values with a Bridge Rectifier using a 15kΩ Resistor As the Load

| # Layers | Turns per Layer | $L_2$ (μH) | | $R_2$ (Ω) | |
|---|---|---|---|---|---|
| | | Predicted | Actual | Predicted | Actual |
| 1 | 20 | 3.27 | 3.02 | 9.84 | 15.0 |

TABLE II. Comparison of Predicted and Observed Values with a Bridge Rectifier using a 15kΩ Resistor As the Load-Continued

| Case | f (MHz) | SRF (MHz) | | $d_{max}$ (mm) | |
|---|---|---|---|---|---|
| | | Predicted | Actual | Predicted | Actual |
| 1 | 4.99 | 37.4 | >30 | 19 | 16 |

Where $d_{max}$ is the distance at which the rectified supply voltage falls below 3.5V, the minimum voltage for proper implant operation.

Next the analytic model was checked using the 16 channel stimulator implant chip for the intracortical visual prosthesis. In the first case, the implant chip drew 0.49mA at 3.5V, and, in the second case, the implant chip drew 0.95mA at 3.5V while in an alternate mode of operation.

TABLE III. COMPARISON OF PREDICTED AND OBSERVED VALUES WITH A THE 16 STIMULATOR IMPLANT AS THE LOAD

| Case | # Layers | Turns per Layer | $L_2$ (μH) | | $R_2$ (Ω) | |
|---|---|---|---|---|---|---|
| | | | Predicted | Actual | Predicted | Actual |
| 1 | 2 | 20 | 13.2 | 15.2 | 29.4 | 27 |
| 2 | 7 | 15 | 89.7 | 82.0 | 413 | ≈91.6 |

TABLE IV. COMPARISON OF PREDICTED AND OBSERVED VALUES WITH A THE 16 STIMULATOR IMPLANT AS THE LOAD- CONTINUED

| Case | f (MHz) | SRF (MHz) | | $d_{max}$ (mm) | |
|---|---|---|---|---|---|
| | | Predicted | Actual | Predicted | Actual |
| 1 | 5.2 | 10.1 | 11.8 | 17.8 | 15.9 |
| 2 | 4.99 | 6.33 | 5.94 | 3.4 | 7.5 |

The decreased accuracy of the second case may be explained by the poor prediction of the ESR by the Dowell Method near resonance due to the change in current distribution in the winding resulting from capacitive effects. This has also been reported elsewhere [31]. The ESR value 91.6Ω for case two was derived from the measurement of impedance at resonance (5.94MHz), which is the series to parallel converted ESR of the coil, $ESR(Q^2+1)$. If this ESR value is used in the calculation of the distance at which the minimum supply voltage is achieved then the new predicted distance is 8mm, which is much closer to that observed.

### *B. Optimization Results*

We optimized the design of the receiver for the Intracortical Visual Prosthesis using the algorithm discussed in section II B. The restrictions imposed were as follows:

Link Level Design Parameters-

$0.5mm \leq$ receiver radius $\leq 2.26mm$

$1 \leq$ number of layers $\leq 20$

$1 \leq$ turns per layer $\leq 20$ (thickness$\leq$0.5mm)

Wire diameter=28.4μm (50AWG)

System Level Design Parameters-

$SRF_{implanted\ coil} \geq f_{carrier}$=5.2MHz

BW≥580kbps

$d_{max} \geq 20mm$

BW≥1.85MHz

where $d_{max}$ is the distance at which the rectified supply voltage falls below $V_{min}$=3.5V for the mode of operation tested.

The optimal coil geometry chosen by the algorithm had 4 layers and 20 layers per turn. A comparison between the predicted and observed results is shown in the table below.

The 16 channel stimulator implant chip for the Intracortical Visual Prosthesis drew as much as 650μA at 3.5V for the mode of operation tested.

TABLE V. VISUAL PROSTHESIS LINK OPTIMIZATION RESULTS

| # Layers | Turns per Layer | $L_2$ (μH) | | $R_2$ (Ω) | |
|---|---|---|---|---|---|
| | | Theor. | Actual | Theor. | Actual |
| 4 | 20 | 51.4 | 50.2 | 134 | 78.0 |

TABLE VI. VISUAL PROSTHESIS LINK OPTIMIZATION RESULTS- CONTINUED

| f | SRF (MHz) | | $d_{max}$ | |
|---|---|---|---|---|
| | Theor. | Actual | Theor. | Actual |
| 5.2 MHz | 5.36 | 6.08 | 20 mm | 22 mm |

Again, with the coil near resonance, the ESR is poorly predicted. With the measured value of ESR, the distance predicted is 22mm. In addition to successfully transmitting power at a distance greater than 20mm, data was also transmitted at a rate of 1.25Mbps.

## IV. CONCLUSION

We conclude that an analytic understanding of a transcutaneous power and outward data link can be used to optimize its system level design parameters using a brute force algorithm. This approach was used to optimize the transcutaneous power and data link for the intracortical visual prosthesis to its requirements without an empirical trial and error approach.

## REFERENCES


[1] Hochberg LR "Neuronal ensemble control of prosthetic devices by a human with tetraplegia," *Nature*, vol. 442, pp. 164–71, 2006.

[2] Kennedy PR "Computer control using human intracortical local field potentials," *IEEE Trans Neural Syst Rehabil Eng*, vol. 12, pp. 339–44, 2004.

[3] Kim, Sung-Phil "Neural control of computer cursor velocity by decoding motor cortical spiking activity in humans with tetraplegia," *Journal of Neural Engineering*, vol 5, pp. 455-476, 2008.

[4] Patil, Parag "Ensemble Recording of Human Subcortical Neurons as a Source of Motor Control Signals for a Brain-Machine Interface," *Neurosurgery*, (2004) vol. 55, pp. 27-38.

[5] Pistohl, Tobias "Prediction of Arm Movement Trajectories from ECoG-Recordings in Humans," *Journal of Neuroscience Methods*, vol. 167, pp. 105-114, 2008.

[6] Schalk G. "Decoding two-dimensional movement trajectories using electrocorticographic signals in humans, " *J Neural Eng*, vol. 4, pp. 264–74, 2007.

[7] Zumsteg, Zachary S. "Power Feasibility of Implantable Digital Spike-Sorting Circuits for Neural Prosthetic Systems," *Proceedings of the 26th Annual International Conference of the IEEE* EMBS, 2004, pp. 4237-240.

[8] Troyk, Philip R. "A 16-Channel Stimulator ASIC for Use in an Intracortical Visual Prosthesis," *10th Annual Conference of the International FES Society*, Jul. 2005.

[9] Raine, C. H. "Skin Flap Thickness in Cochlear Implant Patients - a Prospective Study," *Cochlear Implants Int,*, vol. 8, no. 3, pp. 148-157, Sept. 2007.

[10] Adeloye, Adelola. "Thickness of the Normal Skull in the American Blacks and Whites," *Am. J. Phys. Anthrop.*, vol. 43, no. 1, pp. 23-29, Jul. 1975.

[11] Manola, L. "Modelling motor cortex stimulation for chronic pain control: electrical potential field, activating functions and responses of simple nerve fibre models," *Med. Biol. Eng. Comput*., vol.. 43, no. 3, pp. 335-343, Jun. 2005.

[12] Alturi, Suresh. "Incorporating Back Telemetry in a Full-Wave CMOS Rectifier for RFID and Biomedical Applications," *Proceedings of the IEEE International Symposium on Circuits and Systems ISCAS* (2007): 801-04.

[13] Donaldson, N. "Analysis of Resonant Coupled Coils in the Design of Radio Frequency Transcutaneous Links," *Med. & Biol. Eng. & Comput.*, vol. 21, no. 5, pp. 612-627, Sept. 1983.

[14] Galbraith, Douglas C. "A Wide-Band Efficient Inductive Transdermal Power and Data Link with Coupling Insensitive Gain," *IEEE Transactions on Biomedical Engineering*, vol. 34, no. 4, pp. 265-275, Apr. 1987.

[15] Heetderks, William J. "RF Powering of Millimeter- and Submillimeter-Sized Neural Prosthetic Implants," *IEEE Transactions on Biomedical Engineering*, vol. 35, no. 5, pp. 323-327, May 1988.

[16] Bashirullah, Rizwan. "A Smart Bi-Directional Telemetry Unit for Retinal Prosthetic Device," Proceedings of the 2003 International Symposium on Circuits and Systems, vol. 5, May 2003.

[17] Sácristan-Riquelme, Jordi. "Simple and Efficient Inductive Telemetry System with Data and Power Transmission," *Microelectronics Journal* 39 (2008): 103-111.

[18] Soma, Mani. "Radio-Frequency Coils in Implantable Devices: Misalignment Analysis and Design Procedure," *IEEE Transactions on Biomedical Engineering* 34 (1987): 276-282.

[19] Troyk, P. R. "Class E Driver for Transcutaneous Power and Data Link for Implanted Electronic Devices," *Med. & Biol. Eng. & Comput.*, vol. 30, no. 1, pp. 69-76, Jan. 1992.

[20] Terman, Frederick E. *Radio Engineer's Handbook*. London: McGraw-Hill, 1943.

[21] A B Birtles "Closed form expression for the magnetic field due to a single layer cylindrical coil," *J. Phys. D: Appl. Phys*, vol. 5 1-5 (2005).

[22] E B Rosa : "No 169 – Formulas and Tables for the Calculation of Mutual and Self Inductance," : Scientific Papers of the Bureau of Standards (Third Edition) : December 1916.

[23] Dowell, P.L. "Effects of eddy currents in transformer windings," *Proceedings of the IEEE*, vol. 113, no. 8, pp. 1387–1394, Aug. 1966.

[24] Nan, Xi and Charles R. Sullivan, "An improved calculation of proximity effect loss in high frequency windings of round conductors," in *PESC03*, 2003, vol. 2, pp. 853–860.

[25] Wheeler, Harold A. "Simple Inductance Formulas for Radio Coils," *Proceedings of the IRE*, pp. 1398-1400, Sept. 1928.

[26] Rosa, E.B. : "No 169 – Formulas and Tables for the Calculation of Mutual and Self Inductance," : Scientific Papers of the Bureau of Standards : 1911.

[27] Reuben, Lee, *Electronic Transformers and Circuit.* Wiley, 1947

[28] Ko, Wen "Design of Radio-Frequency Powered Coils for implant instruments, " Medical and Biological Engineering and Computing 1977

[29] Tang, Zhengnian. "Data Transmission from an Implantable Biotelemeter by Load-Shift Keying Using Circuit Configuration Modulator," *IEEE Transactions on Biomedical Engineering* 42 (1995): 524-28.

[30] Kim, Sohee. "Thermal Impact of an Active 3-D Microelectrode Array Implanted in the Brain," *IEEE Transactions on Neural Systems and Rehabilitation Engineering*, vol. 15, pp. 493-501, 2007.

[31] Sullivan, C.R. "Winding Loss Calculation with Multiple Windings, Arbitrary Waveforms and Two-Dimensional Field Geometry," *IEEE Industry Applications Society Annual Meeting*, Oct 1999, pp. 2093-2099